The Astrophysical Journal, 684: L51–L54, 2008 September 1

REALISTIC NUMERICAL SIMULATIONS OF SOLAR CONVECTION AND OSCILLATIONS IN MAGNETIC REGIONS

L. Jacoutot,[1] A. G. Kosovichev,[2] A. Wray,[3] and N. N. Mansour[3]

Received 2008 May 23; accepted 2008 July 22; published 2008 August 13

ABSTRACT

We have used 3D, compressible, nonlinear radiative magnetohydrodynamics simulation to study the influence of magnetic fields of various strengths on convective cells and on the excitation mechanisms of acoustic oscillations by calculating the spectral properties of the convective motions and oscillations. The results reveal substantial changes of the granulation structure with increased magnetic field and a frequency-dependent reduction in the oscillation power in a good agreement with solar observations. These simulations suggest that the enhanced high-frequency acoustic emission at the boundaries of active regions ("acoustic halo" phenomenon) is caused by changes of the spatial-temporal spectrum of turbulent convection in a magnetic field, resulting in turbulent motions of smaller scales and higher frequencies than in quiet-Sun regions.

Subject headings: convection — methods: numerical — Sun: oscillations

1. INTRODUCTION

Observations of solar oscillations have revealed that their properties change significantly in magnetic regions (Braun et al. 1992; Brown et al. 1992). Using *SOHO*/MDI data Hindman & Brown (1998) found that the power of Doppler-velocity oscillations with frequencies less than 5.2 mHz (which corresponds to the acoustic cutoff frequency) decreases with field strength, but the oscillations at higher frequencies become stronger. The regions of enhanced high-frequency oscillation power are usually observed at the boundaries of active regions (outside sunspots) and are sometimes referred as "halos." A similar effect was found for local oscillation modes by Howe et al. (2004), who also found that in magnetic regions the line width of acoustic modes increases at low frequencies and decreases at high frequencies. These variations can be caused by the interaction of acoustic waves with a magnetic field and also by changes in the properties of solar convection and the excitation mechanism of acoustic waves. We address this problem by using realistic numerical simulations of solar convection in the presence of a magnetic field.

2. NUMERICAL MODEL

We use a 3-D, compressible, nonlinear radiative magnetohydrodynamics code developed by A. Wray for simulating the upper solar convection zone and lower atmosphere (Jacoutot et al. 2008). This code takes into account several physical phenomena: compressible fluid flow in a highly stratified medium, radiative energy transfer between the fluid elements, a real-gas equation of state, and magnetic effects. The governing equations are the grid-cell–averaged (henceforth called "averages") conservations of mass (1), momentum (2), energy (3), and magnetic flux (4):

$$\frac{\partial \rho}{\partial t} + (\rho u_i)_{,i} = 0, \tag{1}$$

$$\frac{\partial \rho u_i}{\partial t} + [\rho u_i u_j + (P_{ij} + \rho \tau_{ij})]_{,j} = -\rho \phi_{,i}, \tag{2}$$

$$\frac{\partial E}{\partial t} + \left[E u_i + (P_{ij} + \rho \tau_{ij}) u_j - (\kappa + \kappa_T) T_{,i} + \left(\frac{c}{4\pi}\right)^2 \frac{1}{\sigma + \sigma_T} (B_{i,j} - B_{j,i}) B_j + F_i^{\mathrm{rad}} \right]_{,i} = 0, \tag{3}$$

$$\frac{\partial B_i}{\partial t} + \left[u_j B_i - u_i B_j - \frac{c^2}{4\pi(\sigma + \sigma_T)} (B_{i,j} - B_{j,i}) \right]_{,j} = 0, \tag{4}$$

where ρ is the averaged mass density, u_i is the Favre-averaged velocity, B_i is the magnetic field, and E is the averaged total energy density $E = \rho u_i u_i/2 + \rho e + \rho\phi + B_i B_i/8\pi$, where ϕ is the gravitational potential and e is the Favre-averaged internal energy density per unit mass; F_i^{rad} is the radiative flux, which is calculated by solving the radiative transfer equation, and P_{ij} is the averaged stress tensor $P_{ij} = (p + 2\mu u_{k,k}/3 + B_k B_k/8\pi)\,\delta_{ij} - \mu\,(u_{i,j} + u_{j,i}) - B_i B_j/4\pi$, where μ is the viscosity. The gas pressure p is a function of e and ρ through a tabulated equation of state (Rogers et al. 1996); τ_{ij} is the Reynolds stress, κ is the molecular thermal conductivity, κ_T is the turbulent thermal conductivity, σ is the molecular electrical conductivity, and σ_T is the turbulent electrical conductivity.

For calculations of the eddy viscosity, ν_T, and the Reynolds stress we adopted the most widely used subgrid-scale model of Smagorinsky (1963) in the compressible formulation (Moin et al. 1991). The turbulence model is described in detail by Jacoutot et al. (2008). The turbulent Prandtl number was taken as unity to set κ_T. The molecular viscosity μ and thermal conductivity κ were neglected as their solar values are exceedingly small. The turbulent electrical conductivity σ_T is calculated by using the extension of the Smagorinsky model to the MHD case (Theobald et al. 1994), with the flow velocity shear replaced by a shear of the magnetic field (which is the electric current): $\sigma_T = C_B \Delta^2 |\boldsymbol{j}|$, where $j_i = \epsilon_{ijk} B_{k,j}$ is the resolved elec-

[1] Center for Turbulence Research, Stanford University, Stanford, CA 94305.
[2] Hansen Experimental Physics Laboratory, Stanford University, Stanford, CA 94305.
[3] NASA Ames Research Center, Moffett Field, CA 94035.

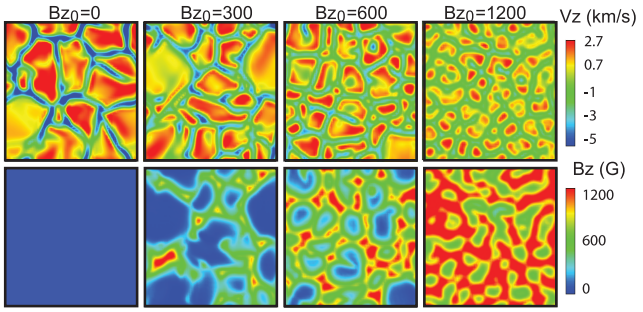

FIG. 1.—Vertical velocity, Vz, and vertical magnetic field, Bz, distributions at the visible surface for different initial vertical magnetic fields, Bz_0.

tric current; ϵ_{ijk} is the Levi-Civita symbol; C_B was taken equal to 1 (Theobald et al. 1994).

We simulate the upper layers of the convection zone using 66 × 66 × 66 grid cells. The region extends 6 × 6 Mm horizontally and from 5.5 Mm below the visible surface to 0.5 Mm above the surface. The initial magnetic field is imposed as a vertical uniform component on a snapshot of the preexisting hydrodynamic convection, calculated as described in Jacoutot et al. (2008). The initial field strength varies from 0 to 1200 G.

3. RESULTS

The first step was to investigate the influence of the initial magnetic field on the granular structure of convection. Figure 1 shows vertical velocity and vertical magnetic field distributions at the visible surface for different magnetic fields. We observe that the size of the granules decreases as the initial magnetic field increases. Without a magnetic field the mean size of granules is about 2 Mm, and it is less than 0.75 Mm for a field of 1200 G. We can also note that the downflow in the intergranular lanes is weaker for strong magnetic fields. Figure 2, which shows the vertical velocity energy as a function of the horizontal wavelength, k_h, measured in degrees of spherical harmonics, $l = k_h R_\odot$, demonstrates this feature. The vertical velocity energy is decreased by a factor of 10^3 for small values of l, which correspond to the larger granules. We can also notice that the magnetic field is swept into the intergranular lanes, although the magnetic field is seeded uniformly. This characteristic of solar magnetoconvection is well-known and has already been presented by Stein & Nordlund (2002) and Cattaneo et al. (2003).

We then studied how the kinetic energy is dissipated for different initial magnetic fields. To do this, we calculated the power spectra of radial modes. Those modes are extracted by

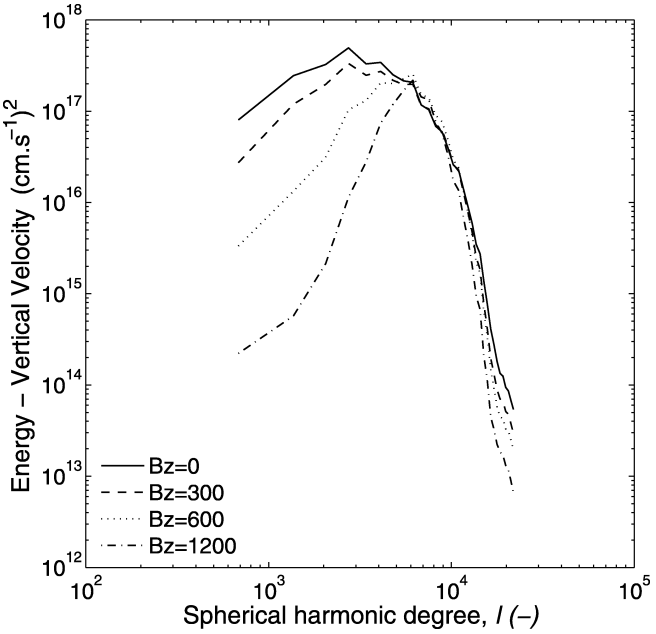

FIG. 2.—Spatial energy of the vertical velocity as a function of the spherical harmonic degree l at the visible surface for different initial vertical magnetic fields.

horizontally averaging the vertical velocity at the solar surface and Fourier-transforming in time. The results are obtained from simulations of 60 hr of solar time using instantaneous snapshots saved every 30 s. In the simulations the oscillation modes appear as broad peaks on top of the flat turbulent convection spectrum (Fig. 3). Five oscillation modes can be clearly seen in the power spectrum. The smallest resonant mode frequency is 2.07 mHz. This mode is excited along all depths. The resonant frequencies supported by the computational box are 2.07, 3.03, 4.10, 5.23, and 6.52 mHz. In addition, several broad high-frequency peaks at 6–12 mHz corresponding to pseudomodes (Kumar & Lu 1991) can be identified. These modes are observed above the acoustic cutoff frequency and are caused by the "source resonance" (Jefferies 1998) rather than by the structural resonance. The source resonance is caused by interference of waves traveling from a subsurface excitation source directly to an observing point at the surface and waves arriving to this point after reflection in deeper layers of the Sun. This effect causes two well-observed phenomena (e.g., Nigam et al. 1998; Mitra-Kraev et al. 2008): asymmetry of the normal-mode peaks and appearance of the high-frequency pseudomodes, both of which are reproduced in the simulations (Fig. 3).

It is clear that the magnetic field significantly affects the

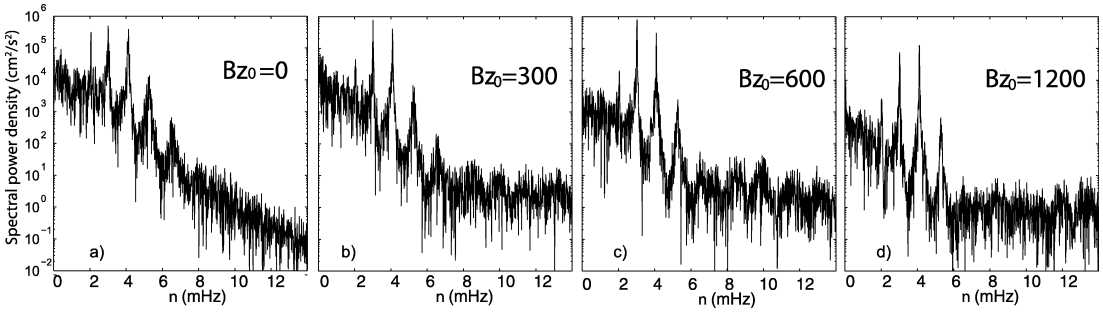

FIG. 3.—Power spectra of the horizontally averaged vertical velocity at the visible surface for different initial vertical magnetic fields. The peaks on top of the smooth background spectrum of turbulent convection represent oscillation modes: the sharp asymmetric peaks below 6 mHz are resonant normal modes, while the broader peaks above 6 mHz, which become stronger in magnetic regions, correspond to pseudomodes.

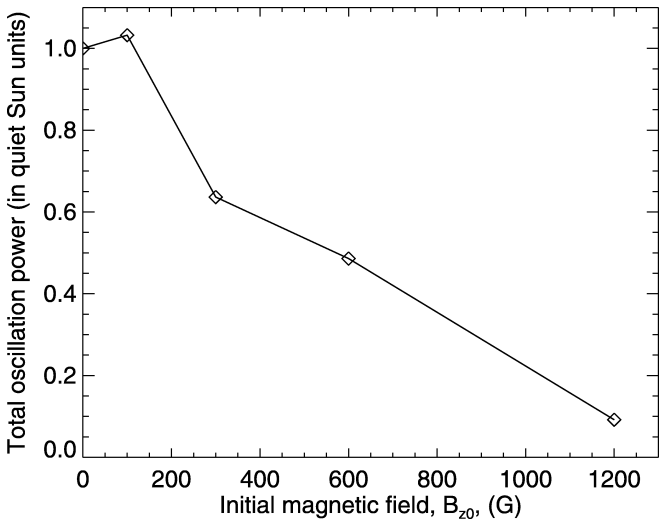

FIG. 4.—Total oscillation power, calculated by summing the oscillation power of the vertical velocity at each point of the domain at the visible surface in the frequency range 1–7 mHz, as a function of initial magnetic field strength.

kinetic energy spectrum. The amplitude of the excited modes decreases as the initial magnetic field increases, as well as the total oscillation power (Fig. 4). The power distribution is shifted toward higher frequencies with the increase of the field strength. It is particularly interesting that the amplitude of the pseudomodes increases with field strength and reaches a maximum at $B_{z0} = 600$ G. This may explain the effect of enhanced high-frequency emission ("acoustic halos") around active regions (Braun et al. 1992; Brown et al. 1992; Hindman & Brown 1998; Jain & Haber 2002). The enhanced emission at frequencies 5–7 mHz appears at the boundaries of magnetic regions outside sunspots, where the magnetic field is moderate. This corresponds to the simulations results: the pseudomode amplitude is high for the 600 G field and diminishes at 1200 G. Each of our simulation boxes represents a small patch of the magnetic regions.

The simulations also show the enhanced spectral power of the convective background at high frequencies for models with magnetic fields, forming plateaus at $\nu > 6$ mHz (Figs. 3*b*–3*d*). This leads to the idea that the high-frequency acoustic halos are caused by enhanced high-frequency turbulent convective motions in the presence of a moderate magnetic field. This is consistent with the decreased granular size in magnetic regions, described in the previous section. The smaller scale convection naturally has higher frequencies and, thus, generates more higher frequency acoustic waves than convection without a magnetic field. When the field is very strong the sound generation decreases because of suppression of convective motions of all scales. This probably explains why the acoustic halos are observed in regions of moderate magnetic field strength at the boundaries of active regions.

In addition, the simulation results show that the modal lines in the oscillation power spectrum (Fig. 3) becomes broader for modes of 2.07 and 3.03 mHz (the first mode almost disappears at $B_{z0} = 1200$ G), but they are more narrow for the modes of 4.10, 5.23, and 6.52 mHz. This qualitatively corresponds to the observational result of Howe et al. (2004). The line asymmetry is also affected by the magnetic field. We note that the power spectrum in Figure 3 is calculated for the surface vertical velocity averaged over the horizontal domain and, thus, represents the oscillations of wavelengths much larger than the size of the domain, 6 Mm, or of the angular degree, $l \ll 700$.

The dominant driving of the *p*-modes comes from the interaction of the nonadiabatic, incoherent pressure fluctuations with the coherent mode displacement. We calculate the mode excitation rate using the method of Nordlund & Stein (2001) but add the contribution of the magnetic pressure $B_k B_k/8\pi$ in the calculation of the total pressure. The rate of energy input to the modes per unit surface area is

$$\Delta\langle E_\omega\rangle/\Delta t = \omega^2 \left| \int_r dr \delta P_\omega^* \left(\partial \xi_\omega/\partial r\right) \right|^2 / 8\Delta\nu E_\omega, \qquad (5)$$

where δP_ω^* is the Fourier transform of the nonadiabatic total pressure; δ in front of the pressure means that one computes so-called pseudo-Lagrangian fluctuations relative to a fixed mass radial coordinate system; $\Delta\nu = \Delta\omega/2\pi$ is the frequency interval for the Fourier transform; ξ_ω is the mode displacement for the radial mode of angular frequency ω; E_ω is the mode energy per unit surface area.

The distributions of the integrand of the work integral as a function of depth and frequency (Fig. 5) are similar to the results obtained by Stein & Nordlund (2001). Most driving is concentrated between the surface and 500 km depth at around 3–4 mHz. We can see that the excitation becomes weaker for a high initial magnetic field. The contribution of the different pressures (gas, turbulent, and magnetic) is presented in Figure 6. The dominant driving comes from the interaction of the coherent mode displacement with the nonadiabatic, incoherent gas pressure fluctuations. The contribution of the turbulent pressure shows similar shape to that of the gas pressure, but it is weaker. The magnetic pressure plays a rather weak role in the excitation of the *p*-modes. However, this contribution becomes higher with increased magnetic field. The total work integrand with increased magnetic field becomes localized closer to the surface and at the mode frequencies.

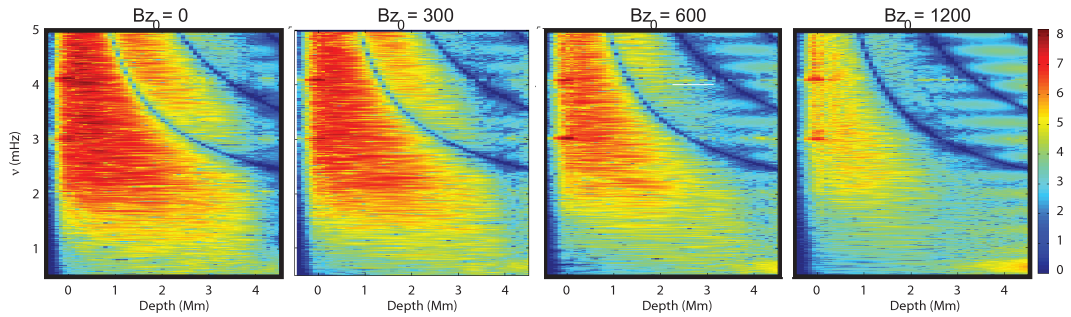

FIG. 5.—Logarithm of the total work integrand (eq. [5] in units of ergs cm^{-2} s^{-1}), as a function of depth and frequency for different initial vertical magnetic field.

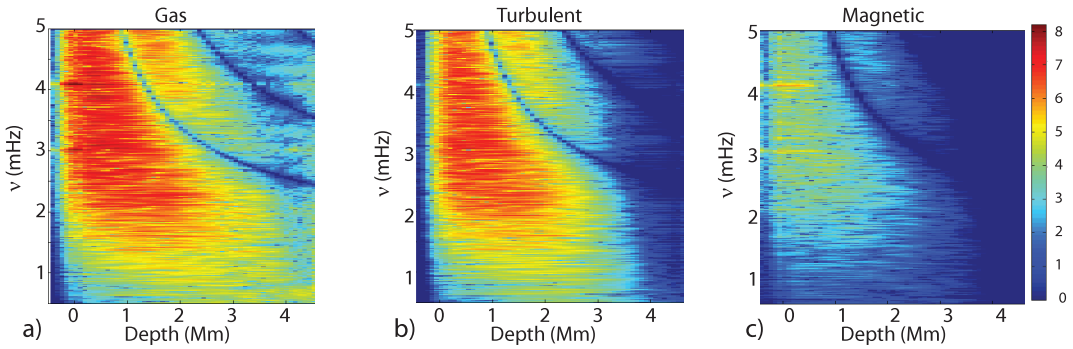

FIG. 6.—Gas, turbulent, and magnetic pressure contributions in the work integrand (in units of ergs cm^{-2} s^{-1}), as a function of depth and frequency for an initial vertical magnetic field of 300 G.

4. CONCLUSIONS

We have carried out realistic simulations of solar convection and oscillation in the presence of magnetic fields of moderate strength. Initially, the magnetic field was vertical and uniformly distributed. The results reproduced several phenomena observed in solar magnetic regions. In particular, the results confirm that the spatial scale of granulation substantially decreases with the magnetic field strength. The magnetic field is swept in the intergranular lanes, and the vertical downdraft motions in these lanes are suppressed. This results is a decrease in the excitation power. The oscillation power in the presence of the magnetic field is shifted toward higher frequencies, also increasing the amplitude of pseudomodes above the acoustic cutoff frequency. At a moderate field strength of ~600 G the power of the high-frequency oscillations reaches a maximum. This corresponds to the "acoustic halo" phenomenon observed in the range of 5–7 mHz in magnetic field areas around active regions outside sunspots. The reason for this phenomenon is probably in the change of the spatial-temporal spectrum of turbulent convection in magnetic fields. The convective motions become smaller in spatial scale and faster in the presence of a magnetic field, and this causes the changes in the oscillations excited by these motions.

The power spectra show a significant increase of the convective power ("plateau") at high frequencies. The increase of the convective power at high frequencies is a likely source of the amplitude increase of high-frequency oscillations. The oscillation modal lines becomes broader and smaller in amplitude for the low-frequencies modes but more narrow at higher frequencies. Qualitatively, this corresponds to the observations but requires a more detailed quantitative study.

The calculations of the work integrand show that the excitation mechanism in magnetic regions of moderate strength remains the same as in the quiet Sun. The oscillations are excited by fluctuations of Reynolds stresses and entropy with magnetic forces playing a minor role. With increased magnetic field the work integrand becomes more concentrated in the near-surface layers and at the mode frequencies.

In general, our simulations suggest that the observed properties of solar oscillations in magnetic regions on the Sun are significantly influenced by changes in the spatial-temporal spectrum of convective motions, which are the source of the oscillations.

REFERENCES

Braun, D. C., Lindsey, C., Fan, Y., & Jefferies, S. M. 1992, ApJ, 392, 739
Brown, T. M., Bogdan, T. J., Lites, B. W., & Thomas, J. H. 1992, ApJ, 394, L65
Cattaneo, F., Emonet, T., & Weiss, N. 2003, ApJ, 588, 1183
Hindman, B. W., & Brown, T. M. 1998, ApJ, 504, 1029
Howe, R., Komm, R. W., Hill, F., Haber, D. A., & Hindman, B. W. 2004, ApJ, 608, 562
Jacoutot, L., Kosovichev, A. G., Wray, A., & Mansour, N. N. 2008, ApJ, 682, 1386
Jain, R., & Haber, D. 2002, A&A, 387, 1092
Jefferies, S. M. 1998, in IAU Symp. 185, New Eyes to See Inside the Sun and Stars (Dordrecht: Kluwer), 415
Kumar, P., & Lu, E. 1991, ApJ, 375, L35
Mitra-Kraev, U., Kosovichev, A. G., & Sekii, T. 2008, A&A, 481, L1
Moin, P., Squires, K., Cabot, W., & Lee, S. 1991, Phys. Fluids A, 3, 2746
Nigam, R., Kosovichev, A. G., Scherrer, P. H., & Schou, J. 1998, ApJ, 495, L115
Nordlund, A., & Stein, R. F. 2001, ApJ, 546, 576
Rogers, F. J., Swenson, F. J., & Iglesias, C. A. 1996, ApJ, 456, 902
Smagorinsky, J. 1963, Mon. Weather Rev., 93, 99
Stein, R. F., & Nordlund, A. 2001, ApJ, 546, 585
———. 2002, in Magnetic Coupling of the Solar Atmosphere (ESA SP-505; Noordwijk: ESA), 83
Theobald, M. L., Fox, P. A., & Sofia, S. 1994, Phys. Plasmas, 1, 9